J Mol Model (2008) 14:1053–1064
DOI 10.1007/s00894-008-0344-6

ORIGINAL PAPER

Modeling the spontaneous initiation of the polymerization of methyl methacrylate

Cuili Zhang · Xueye Wang · Liming Liu · Yanling Wang · Xinyu Peng

Received: 5 March 2008 / Accepted: 20 June 2008 / Published online: 22 July 2008

Abstract The mechanism of the spontaneous initiation of the polymerization of methyl methacrylate (MMA) was investigated theoretically. The six minimum energy paths (MEP) of the possible reactions were calculated using the density functional theory (DFT) in conjunction with the B3LYP functional and 6-31G* basis set. The Diels-Alder initiation mechanism (path (I) and path (II)) with remarkably high energy barriers is not applicable to MMA. Four favorable paths were found (path (III), path (IV), path (V) and path (VI)), which are supporting the Flory mechanism. Path (V) has the lowest active energy. Therefore this path is considered as the main path for the spontaneous polymerization of MMA.

Keywords Density functional theory (DFT) · Intrinsic reaction coordination (IRC) · Methyl methacrylate (MMA) · Spontaneous polymerization

Introduction

Methyl methacrylate (MMA) is one of the most widely used monomers in polymer industry due to its success for producing high molecular weight polymers [1–5]. The studies on spontaneous polymerization of methyl methacrylate (MMA) have introduced both self-initiation and decomposition of impurities [6–13], i.e., oxygen or peroxides in general [14, 15], as the underlying mechanism for the generation of initiating radicals. In a recent study on thermally-initiated MMA polymerization, it is reported that MMA could also undergo reaction with air to form macromolecular peroxides [16–18].

The spontaneous polymerization of styrene is well documented, and the Mayo and Flory mechanisms for the self-initiation of styrene polymerization have been studied using modern computational methods by Kelli S. Khuong and his partners [19]. The Mayo mechanism for styrene cannot be applied to methyl methacrylate (MMA), since the analogous Diels-Alder adducts (DA_1 Pro and DA_2 Pro in Fig. 1) would not have any tendency to homolysis as is the rearomatization in the case of styrene [8]. Therefore, Pryor and Lasswell postulated that a dimeric biradical $\cdot M_2\cdot$ mechanism, proposed in 1937 by Flory for the spontaneous polymerization of styrene and still claimed to be a second minor source of initiating radicals, would be responsible for the initiation in the case of monomers other than styrene [20–22], which gave a simple proof for the existence of the dimeric biradical $\cdot M_2\cdot$ as an intermediate of the initiation mechanism for the spontaneous polymerization of MMA.

So far, the report on the mechanism of the spontaneous initiation of the polymerization of MMA has not systemically appeared in theoretical research. We attempt to conform the Mayo and Flory mechanisms for the spontaneous initiation of the polymerization of MMA, here the quantum chemistry method B3LYP/6-31G* was used to model the process in the gas phase (see Fig. 1).

In this paper, the six possible spontaneous initiation paths were investigated. The potential energy surface information, including the geometries, charges, energies, gradients, and force constants of all the stationary points (reactants, complexes, transition states, and products) and some extra points along the minimum energy path (MEP), was obtained directly from the electronic structure calcu-

C. Zhang · X. Wang (✉) · L. Liu · Y. Wang · X. Peng
Key Laboratory of Environmentally Friendly Chemistry and Applications of Ministry of Education, College of Chemistry, Xiangtan University,
Xiangtan, Hunan 411105, PR China
e-mail: wxueye@xtu.edu.cn

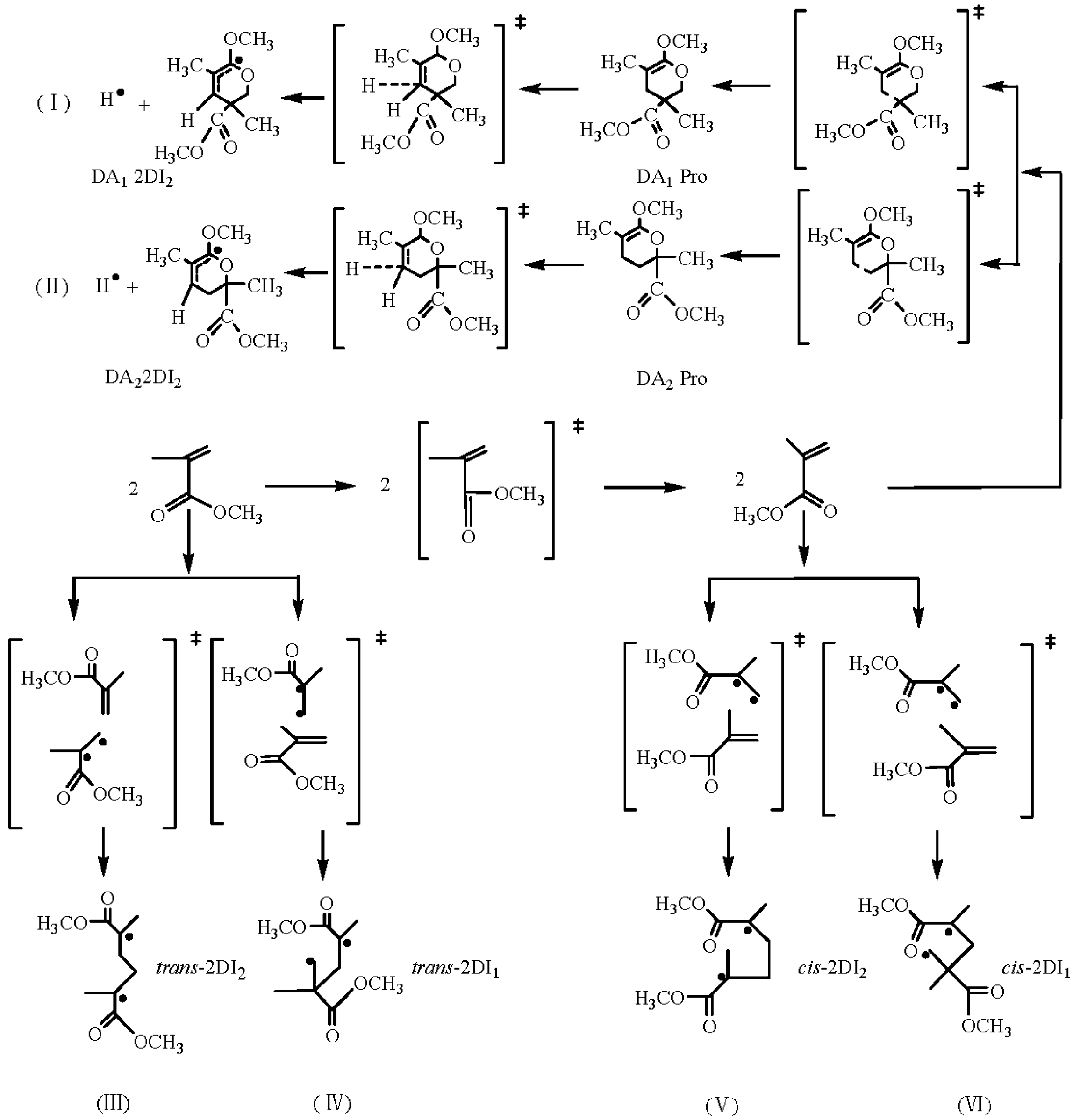

Fig. 1 Possible reaction pathways for the spontaneous initiation polymerization of MMA

lations. The comparison between the theoretical and experimental results was also discussed.

Computational details

For the path (I) and path (II) according to the Mayo mechanism [22, 23], radical initiation firstly proceeds two kinds of Diels-Alder dimerization (see DA_1 Pro or DA_2 Pro in Fig. 1), and then a H atom separates from the DA product generating a H radical and a Diels-Alder radical (see DA_1 2DI or DA_2 2DI in Fig. 1). From path (III) to path (VI) according to the Flory mechanism, two MMA molecules dimerize to form a singlet 1,4-diradical $\cdot M_2 \cdot$ (see *trans*-$2DI_1$, *trans*-$2DI_2$, *cis*-$2DI_1$ and *cis*-$2DI_2$ in Fig. 1). The diradical itself may be capable of initiating the polymerization of MMA.

The density functional theory implemented in the B3LYP hybrid exchange-correlation scheme with spin-unrestricted orbital was used to include some effects of electron correlation. The B3LYP functional employs a three-parameter linear combination of Hartree-Fock exchange, 1988 Becke density gradient correction to exchange, and LYP correction to correlation of Lee [24–26]. It has been successfully applied to many organic and organometallic reactions, giving structures and energies reasonably well. In this work, the geometry optimizations were performed by using the density functional theory

(DFT) [27, 28] and the B3LYP method with the 6-31G* basis set [29] to locate the stationary points on the potential energy surface (PES) [30]. The harmonic vibration frequencies of the stationary points were also determined at the same level to identify the minima or the transition states, i.e., the states when the equilibrium species possess all real frequencies, whereas the transition states possess only one imaginary frequency, and to obtain the zero-point vibration energy (ZPE) corrections. At the same level, the intrinsic reaction coordination (IRC) [31–33] was used to follow the minimum energy paths starting from the transition state until the local minima were reached in the directions of the reactants and the products. All above calculations were carried out by using the Gaussian 03 program [34].

Results and discussions

The six reaction paths were designed for the spontaneous initiation of the polymerization of MMA (see Fig. 1). Path (I) and path (II) are the processes for the formation of DA_1 2DI and DA_2 2DI including a six-member-ring radical and a hydrogen radical. Path (III), path (IV), path (V), and path (VI) generate four kinds of singlet 1,4-diradical ($\cdot M_2 \cdot$).

The *trans*-*cis* MMA is first interconverted by a rotation around the single bond C1–C4 via the transition state *trans*-*cis* TS (a, b, c in Fig. 2). For the path (I), two *cis*-MMA molecules transform into the complexes DA_1C (d in Fig. 2). C5 first bonds with O13 and C4 bonds with C11 generating the Diels-Alder product DA_1 Pro (f in Fig. 2) via the transition state DA_1 TS_1 (e in Fig. 2). And then, the products can lose a H6 radical via a transition state DA_1 TS_2 (g in Fig. 2) which was bonded with C11 producing a π_3^3 radical in the six-member-ring compound. For the path (II), two *cis*-MMA molecules transform into anather complexes DA_2C (i in Fig. 2), C4 firstly bonds with O13 and C5 bonds with C11 generating the Diels-Alder product DA_2 Pro (k in Fig. 2) via the transition state DA_2 TS_1 (j in Fig. 2). And then, the single bond C11–H6 cleaves generating a π_3^3 radical in the six-member-ring and a hydrogen radical (m in Fig. 2) via a transition state DA_2 TS_2 (l in Fig. 2). For path (III) and path (IV), two *trans*-MMA molecules dimerize (tail to tail or tail to head) generating two kinds of biradicals $\cdot M_2 \cdot$ (t and r in Fig. 2) through forming a single bond between C5 and C11 or C4 and C11 by the cleavage of the double bonds C4 = C5 and C9 = C11 via the transition state *trans*-$2DI_2$ TS or *trans*-$2DI_1$ TS (u and s in Fig. 2), respectively. Similarly, two *cis*-MMA molecules can also dimerize (tail to tail or tail to head) generating two kinds of biradicals $\cdot M_2 \cdot$ (p and n in Fig. 2) through forming a single bond between C5 and C11 or C4 and C11 by the cleavage of the double bonds C4 = C5 and C9 = C11 via the transition state *cis*-$2DI_2$ TS or *cis*-$2DI_1$ TS (q and o in Fig. 2), which represent path (V) and path (VI), respectively.

Stationary points along the paths

The spontaneous initiation of the polymerization of MMA in gas phase is multi-steps and multi-paths. The geometries and relative parameters of the reactants, complexes, products, and transition states (TS) on the potential energy surface (PES) of the spontaneous initiation of the polymerization of MMA were found at the B3LYP/6-31G* level, which are displayed in Fig. 2.

The corresponding geometry parameters of *trans*-MMA and *cis*-MMA are close to each other except the dihedral angle between C4 = C5 and C1 = O3 (−180° for the *trans*-MMA and 0° for the *cis*-MMA). For the *trans*-*cis* TS (b in Fig. 2), the corresponding bonds are a little longer than those of the stationary structures while the dihedral angle between C4 = C5 and C1 = O3 is about −90° (the average of −180° and 0°).

Comparing the geometrical parameters of path (I) and path (II), we can find that: 1. The corresponding bonds between the *cis*-MMA and complexes (DA_1C or DA_2C) do not differ significantly within 0.003Å. Among the forming single bonds C5–O13, C4–C11 for DA_1C (d in Fig. 2) and C4–O13, C5–C11 for DA_2C (i in Fig. 2), the distance of C4 and C11 for DA_1C is much longer than that of C5 and C11 for DA_2C by 15.3 percent, whereas the distance of C5 and O13 for DA_1C is a little shorter than that of C4 and O13 with 0.034Å; 2. The corresponding bonds of the transition states DA_1 TS_1 and DA_2 TS_1 (e, j in Fig. 2) involved in the Diels-Alder reaction are all elongated differently. The lengths of C4 = C5, C10 = O13 and C9 = C11 for DA_1 TS_1 are elongated by 6.3 percent, 5.1 percent and 5.0 percent, respectively, while those for DA_2 TS_1 are elongated by 7.3 percent, 3.2 percent and 7.5 percent, respectively. The distances of the forming bonds C5–O13, C9 = C10 and C4–C11 for the DA_1 TS_1 or C4–O13, C9 = C10 and C5–C11 for the DA_2 TS_1 compared to the complexes (DA_1C or DA_2C) are shortened by 45.5 percent, 6.5 percent, 60.2 percent, 33.8 percent, 5.5 and 61.6 percent, respectively; 3. The difference of the corresponding bonds between the two kinds of Diels-Alder addition-compounds DA_1 Pro and DA_2 Pro (f and k in Fig. 2) are within 0.008Å, and the breaking double bonds C4 = C5, C10 = O13 and C9 = C11 for the DA_1 Pro compared to those of the transition state DA_1 TS_1 are elongated by 7.9 percent, 7.0 percent and 7.7 percent, respectively. While those for the DA_2 Pro compared to the transition state DA_2 TS_1 are elongated by 6.9 percent, 9.4 percent and 5.0 percent, respectively. Whereas the forming double bond C9 = C10 and the single bonds C4–C11 and

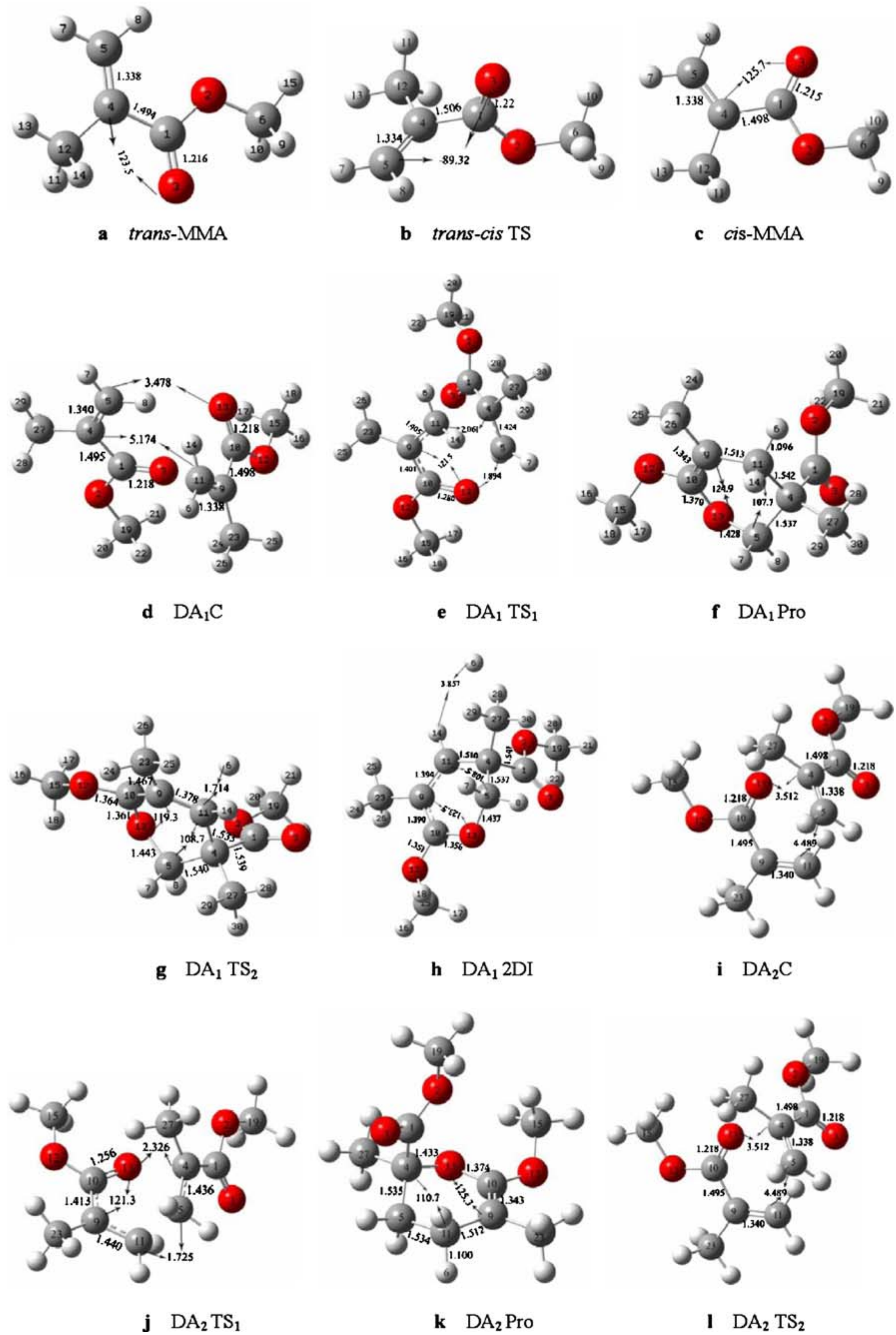

Fig. 2 Geometries optimized at UB3LYP/6-31G* level of theory (Distances are in angstroms, and angles are degrees)

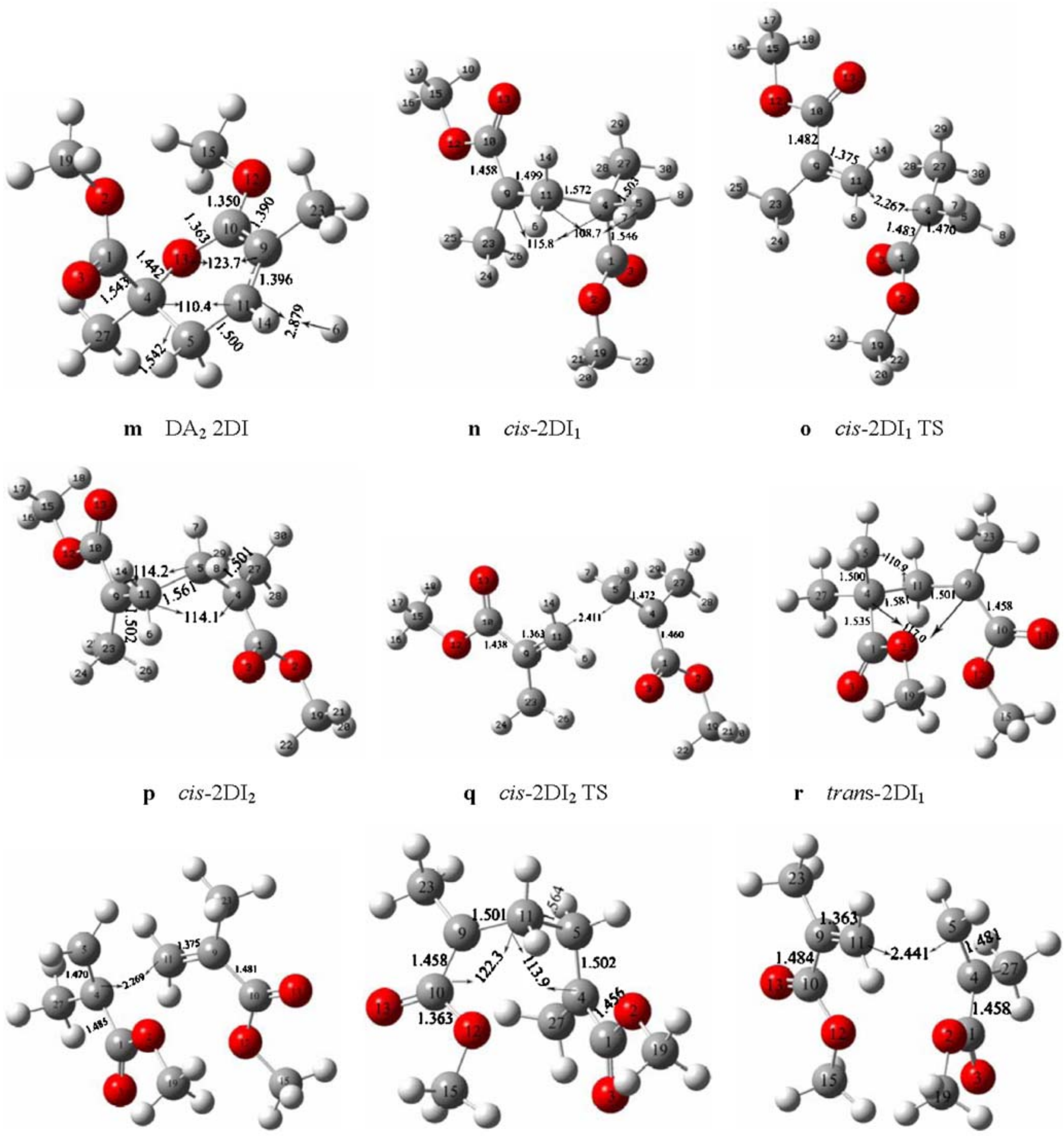

m DA$_2$ 2DI **n** *cis*-2DI$_1$ **o** *cis*-2DI$_1$ TS

p *cis*-2DI$_2$ **q** *cis*-2DI$_2$ TS **r** *trans*-2DI$_1$

s *trans*-2DI$_1$ TS **t** *trans*-2DI$_2$ **u** *trans*-2DI$_2$ TS

Fig. 2 (continued)

C5–O13 for the DA$_1$ Pro compared to those of the transition state DA$_1$ TS$_1$ are shortened by 4.1 percent, 25.2 percent and 24.6 percent, respectively; While the forming double bond C9 = C10 and the single bonds C5–C11, C4–O13 for the DA$_2$ Pro compared to those of the transition state DA$_2$ TS$_1$ are shortened by 5.0 percent, 11.1 percent and 38.4 percent, respectively. The angle of C9, C10 and O13 for the DA$_1$ Pro (124.9°) is a little bigger than that of the corresponding transition state DA$_1$ TS$_1$ (121.5°), while that of the DA$_2$ Pro (125.3°) is a little bigger than that of the corresponding transition state DA$_2$ TS$_1$ (121.3°). From above, we can find that the transition states are a little product-like, both the bonds and angles are close to the DA products; 4. The following transition states producing two individual radicals (g and l in Fig. 2) have different location in the double bond, which are located on the C9 and C11 compared to the DA products located on C9 and C10, and the radical of the six-member ring compound is located on C10 bonded to two O atoms which can attract the single electron. For the six-member ring radical products with a hydrogen radical DA_1 2DI and DA_2 2DI (h and m in Fig. 2), the C10, C9 and C11 can form a π_3^3 bond stabilizing the six-member ring radical. Compared to the corresponding Diels-Alder addition-compounds DA_1 Pro and DA_2 Pro (f and k in Fig. 2), the angles of C9, C10 and O13 become a little smaller for the following transition states DA_1 TS_2 and DA_2 TS_2, but get a little bigger for the six-member ring radical products. Whereas the angles of C5, C4 and C11 for the transition states DA_1 TS_2 and DA_2 TS_2 (g and l in Fig. 2) become a little bigger, but get a little smaller for the six-member ring radical products (h and m in Fig. 2). The distance of C11 and H6 are elongated gradually from the Diels-Alder addition-compounds to the six-member ring radical products.

The geometrical parameters of the stationary points along the path (III), path (IV), path(V) and path (VI) have some similarities: 1. Two MMA molecules dimerize into four kinds of singlet 1,4-diradical ($\cdot M_2 \cdot$) via the transition states *trans*-$2DI_2$ TS, *trans*-$2DI_1$ TS, *cis*-$2DI_2$ TS and *cis*-$2DI_1$ TS (u, s, q, and o in Fig. 2), respectively; 2. All the dimerization transition states include a biradical located on the atoms of C4 and C5 from the double bond C4 = C5 and a MMA molecule having some changes compared to the original MMA; 3. The dimerization biradicals $\cdot M_2 \cdot$ *trans*-$2DI_2$, *trans*-$2DI_1$, *cis*-$2DI_2$ and *cis*-$2DI_1$ (t, r, p, and n in Fig. 2) are all transformed through forming a single bond between C4 and C11 or C5 and C11 by the cleavage of the double bonds C4 = C5 and C9 = C11 asynchronously. In the reaction process, the involved bonds are changed differently compared to the original MMA molecules: For path (III), the distances of C9 and C11, C5 and C4 for the dimerization transition state *trans*-$2DI_2$ TS are elongated by 1.9 percent, 10.7 percent, respectively, while for the dimerization product *trans*-$2DI_2$ are elongated by 12.2 percent, 12.3 percent, respectively. The distance of C5 and C11 is shortened by 35.9 percent for the dimerization product *trans*-$2DI_2$ compared to the dimerization transition state *trans*-$2DI_2$ TS. For the path (IV), the distances of C9 and C11, C5 and C4 for the dimerization transition state *trans*-$2DI_1$ TS are elongated by 2.8 percent and 9.9 percent, respectively, while for the dimerization product *trans*-$2DI_1$ are elongated by 12.2 percent and 12.1 percent, respectively. The distance of C4 and C11 is shortened by 30.3 percent from the dimerization transition state *trans*-$2DI_1$ TS to the dimerization product *trans*-$2DI_1$. For the path (V), the distances of C9 and C11, C5 and C4 for the dimerization transition state *cis*-$2DI_2$ TS are elongated by 1.9 percent, 10.0 percent, respectively, while for the dimerization product *cis*-$2DI_2$ are elongated by 12.3 percent, 12.2 percent, respectively. The distance of C5 and C11 is shortened by 35.3 percent from the dimerization transition state *cis*-$2DI_2$ TS to the dimerization product *cis*-$2DI_2$. For the path (VI), the distances of C9 and C11, C5 and C4 for the dimerization transition state *cis*-$2DI_1$ TS are elongated by 2.8 percent, 9.9 percent, respectively, while for the dimerization product *cis*-$2DI_1$ are elongated by 12.0 percent, 12.3 percent, respectively. The distance of C4 and C11 is shortened by 30.7 percent for the dimerization transition state *cis*-$2DI_1$ TS compared to the dimerization product *cis*-$2DI_1$.

Charges of the stationary points

Although the absolute values of the atomic charges are considered to have little physical meaning, their relative values can give some useful information. A lower electron density yields a lower reactivity, whereas a higher electron density yields a higher reactivity. The Mulliken charges for the correlative reaction positions (C4, C5, C9, C11, O13, H6) of the stationary points (see Fig. 2) are listed in Table 1. C4, C5, C9 and C11 are all on the double bonds, where C5 and C11 are the tail-Carbons; O13 is the oxygen atom which can bond with C4 or C5 in the Diels-Alder reaction; H6 is the hydrogen atom which may separate from the Diels-Alder product.

In the *trans-cis* transformation process, the Mulliken charges on C4 of the *trans*-MMA (0.129) and *cis*-MMA (0.130) are very close with the difference of 0.001, but which is much higher for the transition state *trans-cis* TS (0.166) than the stationary points; The Mulliken charges on C5 are all negative for the three species, and for the *trans-cis* TS (−0.365), C5 obtains higher electron density than that of *cis*-MMA (-0.358) and lower than that of *trans*-MMA (−0.370). The above indicates that the C5 on the stationary points has very high reactivity.

For path (I), the Mulliken charges on C5, O13 and C11 are all negative for five species. The electron density of C11 decreases in turn from −0.365 for DA_1C to −0.217 for DA_1 2DI. To C5, the electron density decreases obviously from DA_1C (−0.381) to DA_1 Pro (−0.017) in turn, and then increases a little for DA_1 TS_2 (−0.047) and decreases a little again for the DA_1 2DI (−0.034). But for O13, the electron density changes ruleless within 0.048, and the O13 on DA_1 TS_1 (−0.525) points to the highest electron density but for DA_1 TS_2 (−0.481) points to the lowest. The Mulliken charges on C4 for DA_1C (0.130) is positive but for the others are all negative, whereas the property of the Mulliken charges on C9 of the five species are in

Table 1 Predicted Mulliken charges of the stationary points at the B3LYP/6-31G* level

Species	C4	C5	C9	C11	O13	H6
trans-MMA	0.129	−0.370	——	——	——	——
cis-MMA	0.130	−0.358	——	——	——	——
trans-cis TS	0.166	−0.365	——	——	——	——
DA_1C	0.130	−0.381	−0.141	−0.365	−0.512	——
DA_2C	0.141	−0.366	0.130	−0.381	−0.500	——
DA_1 TS_1	−0.033	−0.179	0.099	−0.356	−0.525	——
DA_2 TS_1	0.162	−0.373	0.101	−0.345	−0.526	——
DA_1 Pro	−0.071	−0.017	0.071	−0.327	−0.509	0.163
DA_2 Pro	0.217	−0.274	0.075	−0.340	−0.532	0.157
DA_1 TS_2	−0.016	−0.047	0.134	−0.256	−0.481	−0.086
DA_2 TS_2	0.222	−0.276	0.155	−0.250	−0.511	−0.088
DA_1 2DI	−0.072	−0.034	0.129	−0.217	−0.502	0.002
DA_2 2DI	0.217	−0.295	0.131	−0.204	−0.523	−0.021
trans-$2DI_1$ TS	0.022	−0.334	0.137	−0.403	−0.497	——
trans-$2DI_2$ TS	0.106	−0.351	0.122	−0.383	−0.492	——
cis-$2DI_1$ TS	0.031	−0.331	0.133	−0.401	−0.508	——
cis-$2DI_2$ TS	0.094	−0.357	0.117	−0.356	−0.510	——
trans-$2DI_1$	−0.001	−0.311	0.118	−0.349	−0.503	——
trans-$2DI_2$	0.109	−0.326	0.102	−0.331	−0.501	——
cis-$2DI_1$	−0.007	−0.305	0.091	−0.346	−0.504	——
cis-$2DI_2$	0.094	−0.326	0.095	−0.326	−0.506	——

the reverse trend. H6 is involved in DA_1 Pro, DA_1 TS_2 and DA_1 2DI, the obtained Mulliken atomic charges are 0.163, −0.086 and 0.002, respectively, which shows that H6 tends to be electric neutrality. We can conclude that: With the reaction proceeding, the Mulliken charges on C5 and C11 transfer to other atoms of the reaction system, i.e., C4 and H6, and the corresponding reactivity decrease somewhat; While the electron density of O13 changes very little.

For path (II), the Mulliken charges on C5, O13 and C11 are all negative for the five species from DA_2C to DA_2 2DI. The electron density of C11 decreases in turn from −0.381 to −0.204, just as path (I). To C5, the electron density firstly increases a little from DA_2C (−0.366) to DA_2 TS_1 (−0.373) and then decreases a little to DA_2 Pro (−0.274), and increases again till DA_2 2DI (−0.295). But for O13, the electron density firstly increases from DA_2C (−0.500) to DA_2 Pro (−0.532), and then decreases a little to DA_2 TS_2 (−0.511), and increases a little again to DA_2 2DI (−0.523). The Mulliken charges on C4 and C9 are all positive. The electron density on C4 increases slightly in turn from DA_2C (0.141) to DA_2 TS_2 (0.222), and then decreases a little to DA_2 2DI (0.217), which is equal to that of DA_2 Pro. Whereas the Mulliken charge on C9 first decreases from DA_2C (0.130) to DA_2 Pro (0.075), and then increases a little to DA_2 TS_2 (0.155), and decreases a little again to DA_2 2DI (0.131), which is just the opposite to the changes of O13. H6 is involved in DA_2 Pro, DA_2 TS_2 and DA_2 2DI, the obtained Mulliken atomic charges are 0.157, −0.088 and −0.021, respectively, which is close to path (I). We can conclude that: With the reaction proceeding, the Mulliken charges on C5 and C11 transfer to other atoms of the reaction system, i.e., H6, just as path (I). The H6 also tends to be electric neutrality; While the electron density of O13 changes very little and keeps quite high, which indicates the O13 atom is instable in this compounds.

For path (III), the Mulliken charges on C5 and C11 both decrease some from *trans*-MMA to *trans*-$2DI_2$. The electron density of C4 and C9 are both with some decrease compared to the C4 of the original *trans*-MMA, and always keeps positive with the slight difference within 0.016. The Mulliken charges on O13 are all negative for the compounds involved, and for the *trans*-$2DI_2$ (−0.501) is a little higher than the *trans*-$2DI_2$ TS (−0.492). We can also conclude that, with the reaction proceeding, the Mulliken charges on C5 and C11 transfers to other atoms of the reaction system, i.e., C4 and C9, and the two radicals may locate on them which can be more stable.

For path (IV), the Mulliken charge on C5 decreases obviously from *trans*-MMA (−0.370) to *trans*-$2DI_1$ (−0.311). The electron density of C11 for the transition state *trans*-$2DI_1$ TS (−0.403) reaches the highest, which is the lowest for the *trans*-$2DI_1$. The electron density of C4 decreased obviously from original *trans*-MMA (0.129) to the biradical M_2 *trans*-$2DI_1$ (−0.001) tends to electric neutrality. The Mulliken charges of C9 are all positive for the three species, and the electron density of the transition state is a little higher than the others. We can also conclude that: With the reaction proceeding, the Mulliken charge on

C5 and C11 transfers to other atoms of the reaction system, i.e., C4 and C9, just as path (III). The two radicals may locate on C5 and C9, which can be more stable.

For path (V), the Mulliken charge on C5 decreases a little from *cis*-MMA (−0.358) to *cis*-$2DI_2$ (−0.326). The electron density of C11 for the transition state *cis*-$2DI_2$ TS (−0.356) is a little lower than that of the tail-carbon C5 of original *cis*-MMA and a little higher than that of the biradical $\cdot M_2\cdot$ *cis*-$2DI_2$ (−0.326). For the biradical $\cdot M_2\cdot$, the electron density of C11 is nearly equal to C5, which indicates the reactivity of the two carbon atoms is equal. While the electron density of C4 decreased obviously from the original *cis*-MMA (0.130) to the *cis*-$2DI_2$ TS (0.094) equal to that of the biradical $\cdot M_2\cdot$ *cis*-$2DI_2$. The Mulliken charges of C9 are both positive for the *cis*-$2DI_2$ TS (0.117) and *cis*-$2DI_2$ (0.095), and the former is a little higher. At the same time, the electron density of C4 and C9 are very close for the biradical $\cdot M_2\cdot$. We can also conclude that: With the reaction proceeding, the Mulliken charge on C5 and C11 transfers to other atoms of the reaction system, i.e., C4 and C9; 2. The reactivity of C5 and C9 is nearly the same; 3. The reactivity of C4 for the transition state, the *cis*-$2DI_2$ and C9 for the *cis*-$2DI_2$ is resembling.

For path (VI), the Mulliken charges on C4 and C5 decrease in order, while the former is more obvious. The electron density on C11 for the transition state *cis*-$2DI_1$ TS (−0.401) is higher than the stationary points, while that for the *cis*-$2DI_1$ is the lowest, just as path (IV). The Mulliken charges of C9 are all positive for three states, and electron density of the transition state is the highest, while that for the *cis*-$2DI_1$ is the lowest. Comparing path (V) and path (VI), we can find that the Mulliken charge on O13 for both paths keeps almost the same, and that of C9 for cis-$2DI_1$ and $2DI_2$ are close to each other.

From the discussion above we can find that: The charge of O13 for all the compounds always keeps negative with quite high electron density. The reactivity of the same atoms for path (III) and path (V), path (IV) and path (VI) has some resembling, respectively.

Relative energies

The predicted imaginary frequencies for transition states (TS), zero point energies *ZPE*, single-point energies *E* for all species, the relative energies E_{rel} with the *ZPE* correction and E_{rel}' without the *ZPE* correction for different reactions are shown in Table 2. It was found that every transition state (TS) has only one imaginary vibrational frequency. It indicates that the designed reactions may be confirmed.

Comparing the relative energies E_{rel} with the *ZPE* correction and E_{rel}' without the *ZPE* correction, the values are very close, except for the DA_1 Pro, DA_1 TS_2 and DA_2 2DI in the Diels-Alder process with the difference of 8.6 percent, 3.0 percent and 5.1 percent, respectively, whereas for the demerization paths the differences is very little

Table 2 Predicted imaginary frequency (for TS), *ZPE* (Hatree), single-point energies *E* (Hatree), and relative energies *E*rel (kJ/mo1) at the B3LYP/6-31G* level

Species	Imaginary frequency	*ZPE*	*E*	E_{rel} (with ZPE correction)		E_{rel}' (without ZPE correction)
2 *trans*-MMA		0.2432	−691.5734	0		0
2 *cis*-MMA		0.2432	−691.5730	0.8612		0.8664
2 *trans*-*cis* TS	−80i	0.2432	−691.5538	48.41		48.37
DA_1C		0.244056	−691.5780	−9.965		−9.919
DA_2C		0.244090	−691.5780	−9.864		−9.819
DA_1 TS_1	−575i	0.245392	−691.5176	152.1		152.2
DA_2 TS_1	−210i	0.245242	−691.5300	119.1		119.2
DA_1 Pro		0.249672	−691.5727	18.67		17.06
DA_2 Pro		0.249310	−691.5782	3.266		3.576
DA_1 TS_2	−1273i	0.243985	−691.4103	430.0		417.3
DA_2 TS_2	−1151i	0.238777	−691.4203	390.2		390.0
DA_1 2DI		0.236623	−691.4355	344.7		344.4
DA_2 2DI		0.236156	−691.4318	353.0		335.9
Trans-$2DI_1$ TS	−433i	0.239540	−691.4703	260.8		260.6
cis-$2DI_1$ TS	−430i	0.239806	−691.4726	255.7		255.5
Trans-$2DI_2$ TS	−353i	0.240055	−691.4728	255.7	226 [13]	255.6
cis-$2DI_2$ TS	−290i	0.240252	−691.4760	248.3		248.2
Trans-$2DI_1$		0.242664	−691.5056	176.3		176.3
cis-$2DI_1$		0.242980	−691.5077	171.9		171.9
Trans-$2DI_2$		0.244908	−691.5340	107.8	142 [13]	107.9
cis-$2DI_2$		0.244651	−691.5340	107.2		107.2

within 0.2kJ/mol. In the following discussion, the relative energies with the *ZPE* correction E_{rel} was used.

Table 2 shows that the energy barrier for the *trans-cis* transition of MMA is rather small (only 24.2kJ/mol), and the energy barriers for the six paths are about 430kJ/mol, 390kJ/mol, 255.7kJ/mol, 260.8kJ/mol, 248.3kJ/mol and 255.7kJ/mol, respectively. We can conclude that the active energies for different reaction path are in the following order: path (I)>path (II)>>path (IV)>path (III)=path (VI)>path (V).

In the Diels-Alder reaction process, the Mulliken charges of the involved atoms C11 and O13 for the transition states DA_1 TS_1 and DA_2 TS_1 differ slightly within 0.011. While compared to the original *cis*-MMA, those of C4 and C5 for the transition state DA_1 TS_1 decrease with 0.163 and 0.179, respectively. But for the DA_2 TS_1, those of C4 and C5 increase with 0.032 and 0.015, which transfers much less charges than the DA_1 TS_1 (see Table 1). In the process of the formation of the six-member ring radical with a H radical, the Mulliken charges on the involved atoms C11 and H6 of the transition states DA_1 TS_2 and DA_2 TS_2 differ slightly within 0.006; While for the Diels-Alder addition products, the Mulliken charge of H6 for DA_1 Pro (0.163) is higher than DA_2 Pro (0.157), whereas the Mulliken charge on C11 for the DA_1 Pro (−0.327) is much lower than DA_2 Pro (−0.340), see Table 1. In a word, path (I) need transfer more charges than path (II), which may cause the higher energy barrier for path (I) compared to path (II).

The energy barriers for path (I) and path (II) are far higher than the other four paths. For path (I) and path (II), the energy barriers include two parts which are the Diels-Alder reaction and the formation of the six-member ring radical products. The process refers to the cleavage of three double bonds (C9 = C11, C10 = O13 and C4 = C5) and one single bond (C11–H6), the formation of a π_3^3 radical (C10-C9-C11) in the six-member-ring and two single bonds (C4–C11 and C5–O13 for the path (I), or C5–C11 and C4–O13 for path (II)). For the other four paths, the energy barriers are only for the formation of the dimerization biradical $\cdot M_2\cdot$. The process refers to the cleavage of two double bonds (C9 = C11 and C4 = C5), and the formation of the singlet 1,4-diradical $\cdot M_2\cdot$.

The dimerization of *cis*-MMA is much easier than that of the *trans*-MMA, which may the steric hindrance brought by the relative position of two MMA molecules (see o, q, s and u in Fig. 2). The energy barriers for the tail to tail $\cdot M_2\cdot$ biradical are a little lower than the tail to head $\cdot M_2\cdot$ biradical, i.e., the energy barrier for the formation of *trans*-$2DI_1$ is a little higher than that of the *trans*-$2DI_2$ with 5.1kJ/mol, while the energy barrier for the formation of *cis*-$2DI_1$ is also a little higher than that of the *cis*-$2DI_2$ with 7.4kJ/mol. It may be the steric hindrance brought by methyl group located on the C4 causing in some difficulty for another group to attack.

The predicted activation energy obtained in our work is much higher than ref. [13], which is 226kJ/mol for a monomer biradical just as the transition states *trans*-$2DI_2$ TS (255.7kJ/mol) and *cis*-$2DI_2$ TS (248.3kJ/mol) in this paper with the difference of 13.1 percent and 9.8 percent, respectively. While the reaction energy for the *trans*-$2DI_2$ (107.8kJ/mol) and *cis*-$2DI_2$ (107.2kJ/mol) in this work are much lower than that of the Sticker M's work with 24.1 percent and 24.5 percent, respectively. The predicted energies in our work are in some accordance with the former work.

From the discussion above, some conclusions can be made: 1. The relative energies E_{rel} with the *ZPE* correction and E_{rel}' without the *ZPE* correction are close, except for the DA_1 Pro, DA_1 TS_2 and DA_2 2DI belonging to the Diels-Alder process; 2. In the forming of the dimer biradicals $\cdot M_2\cdot$, there are four transition states located by the B3LYP/6-31G* method, and they are all endothermic process. With temperature rising without the initiator, the dimerization of the MMA can proceed; 3. The radical coming from the Diels-Alder reaction is not thermodynamically favorable path, which proves the Flory mechanism for the spontaneous initiation of the polymerization of MMA; 4. The biradical paths are the major paths in the spontaneous initiation of the polymerization of MMA in gas phase.

MEPs along the reaction paths

Since finding one imaginary frequency (saddle point) does not guarantee that one has found a transition structure that is involved in the reaction paths, each transition state optimized structure was submitted for intrinsic reaction coordinate (IRC, minimum energy path) calculations. Although saddle points (transition states) generally connect two minima on the PES, these minima may not be the structures of interest [35–39]. An IRC calculation examines the reaction path leading down from a transition structure on a PES. The calculation starts at the saddle point and follows the reaction in both directions. Thus, the IRC calculations definitively connect two minima on the PES by a path that passes through the transition state between them. However, two minima on a PES may have more than one reaction path connecting them, corresponding to different transition structures through which the reaction passes [40].

The MEPs for the six paths were calculated by the intrinsic reaction coordination (IRC) theory at the UB3LYP/6-31G* level (see Fig. 3). (i) is the IRC for the *trans-cis* MMA transform process. (ii) is the IRC for the formation of the Diels-Alder addition product DA_1 Pro of the path (I), but we cannot obtain the following IRC for the formation of DA_1 2DI, which indicates that the path (I) cannot occur in the spontaneous initiation process of MMA. In the former

Fig. 3 IRC for the spontaneous initiation polymerization of MMA at the B3LYP/6-31G* level

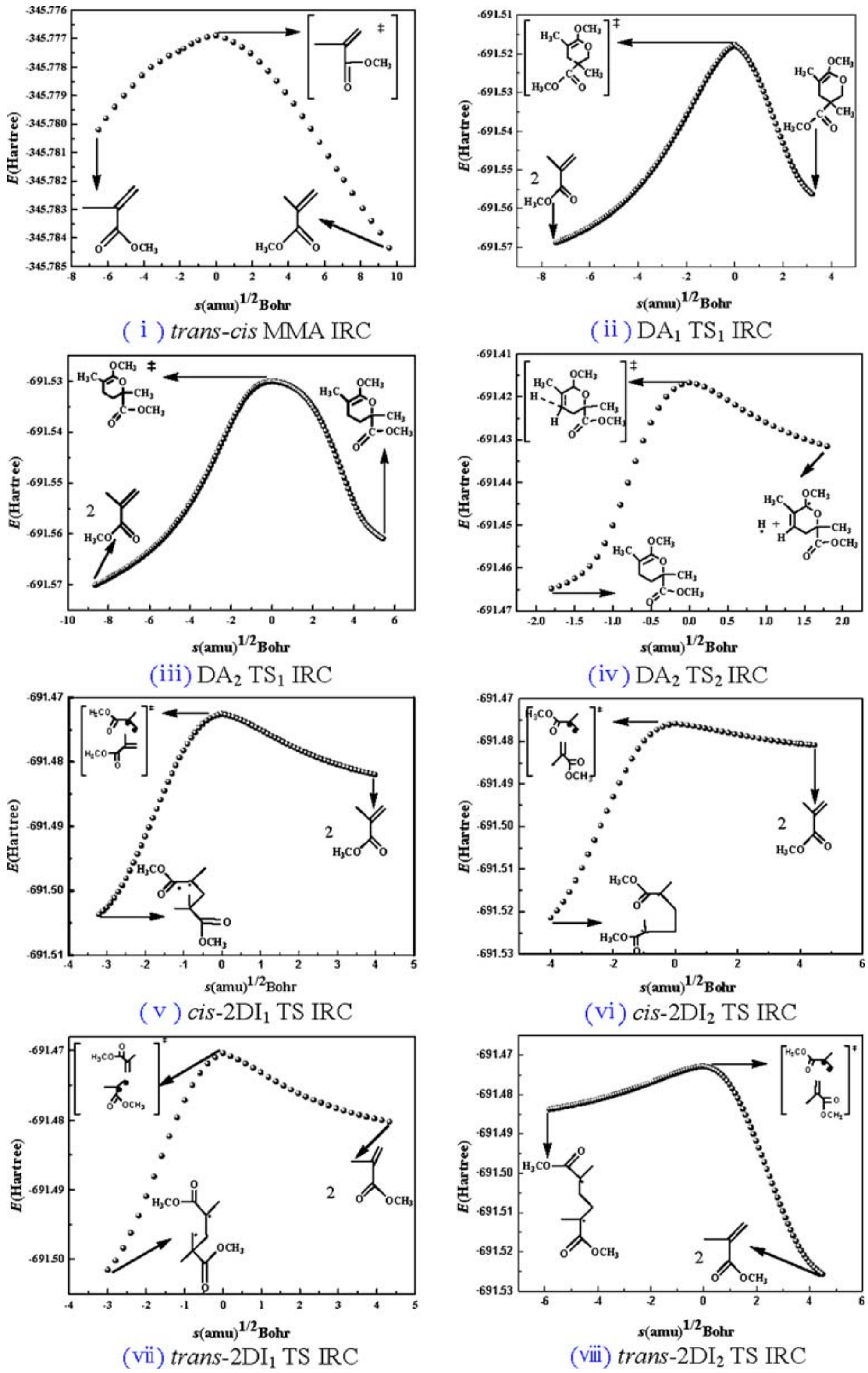

part *Relative energies*, the active energy of the path (I) reaches 430kJ/mol, which is the highest among the six paths. The IRC analysis strongly support the energy results. (iii) and (iv) are the IRC for the path (II), the former is for the formation of the Diels-Alder addition product DA_2 Pro, and the latter is for the formation of the six-member-ring radical with a H radical process; (v) is the IRC for the path (VI); (vi) is the IRC for the path (V); (vii) is the IRC for the path (IV); (viii) is the IRC for the path (III). They illustrate a change in energy and snapshots of the reacting system

Table 3 Activation parameters for the spontaneous initiation polymerization of MMA

Reaction	$\Delta H^{\neq}$ (kJ/mo1)		$\Delta S^{\neq}$ (J/mol·K)		$\Delta G^{\neq}$ (kJ/mo1)
trans-MMA→*cis*-MMA	19.22		−15.84		28.65
DA_1C→DA_1 Pro	154.1		−90.1		207.8
DA_2C→DA_2 Pro	120.3		−82.7		169.7
DA_1 Pro→DA_1 2DI	397.3		4.711		394.4
DA_2 Pro→DA_2 2DI	318.7		22.5		305.3
2 *trans*-MMA→*trans*-$2DI_1$	254.6		−151.2		344.8
2 *cis*-MMA→*cis*-$2DI_1$	248.9		−154.3		340.9
2 *trans*-MMA→*trans*-$2DI_2$	250.6	226 [13]	−146.2	−178 [13]	337.8
2 *cis*-MMA→*cis*-$2DI_2$	243.1		−133.1		322.5

along the IRC, and validate the existence of the transition states obtained from the calculation.

Thermal parameters

The values for the activation enthalpy $\Delta H^{\neq}$, activation entropy $\Delta S^{\neq}$ and activation Gibbs free energy $\Delta G^{\neq}$ are presented in Table 3. It can be seen that all the activation enthalpy for the six paths are positive, thus represent an endothermic process for the formation of the transition states and need energy from environment to initiate the reaction, which is consistent with ref. [13]. From Table 3, the active enthalpies for six paths are 397.3 kJ/mol, 318.7 kJ/mol, 250.6 kJ/mol, 254.6 kJ/mol, 243.1 kJ/mol and 248.9 kJ/mol, respectively. It is easy to find the activation enthalpies for different reaction paths are in the following order: path (I)>path (II)>>path (IV)>path (III)>path (VI)>path (V), which is very similar to the order of the active energy except for a little difference between the path (III) and path (VI).

According to Flory and Sticker [13,21], the *E*a values directly correspond to the $\Delta H^{\neq}$ values for the formation of the biradical as calculated according to Hess' Law [41]. In Sticker' paper, it needs 226 kJ/mol energy for the formation of a monomer biradical just as the transition states of the dimerization in work, which include a monomer biradical and a MMA molecule with some changes compared to the original MMA [13]. The value is much lower than the present work by about 12.4 percent at most.

The order also proves the above conclusions in the *Relative energies* section: 1. The Diels-Alder reaction is not the thermodynamically favorable path, which proves the Flory mechanism for the spontaneous initiation of the polymerization of MMA again; 2. The forming of dimeric biradicals $\cdot M_2 \cdot$ are all endothermic process, if supporting proper energy without the initiator, the dimerization of the MMA can proceed; 3. The biradical paths are the major paths in the spontaneous initiation of the polymerization of MMA in gas phase.

The active entropy change in most of the spontaneous initiation of the polymerization of MMA (for the path (III), path (IV), path (VI) and path (V)) is always negative because the reactions are two MMA moleculars dimerize into one biradicals $\cdot M_2 \cdot$ accompanied by the reduction of freedom degree. But for path (I) and path (II), the Diels-Alder reaction process is two *cis*-MMA molecules transforming into a molecule (DA_1 Pro or DA_2 Pro) with the reduction of freedom degree, while the following is the DA product loses a H radical and forms a six-member-ring radical, with the increase of freedom degree. The calculated results are in a good agreement with the experimental data (−178 J/mol·K) for the polymerization [13], which is a little lower than this work with 25 percent at most.

Conclusions

In the present work, the six possible paths for the spontaneous initiation of the polymerization of MMA were studied with the quantum chemistry method. We have studied this system through the analysis of the geometries, the charges, the relative energies, the MEPs along the reaction paths and the thermal parameters involved in the reactions we designed. The methodology used has proved satisfactory to provide an understanding of the spontaneous initiation of the polymerization of MMA. From the above study the following conclusion can be made: 1. The Diels-Alder initiation mechanism has the highest energy barrier which is not applicable to MMA, just as proposed in ref. [8]. 2. Except the tail to tail addition reaction, the tail to head addition reaction can also proceed, and four kinds of biradicals $\cdot M_2 \cdot$ are found. 3. The *cis*-MMA via tail-tail demerization is the most favorable path among the last four paths for the spontaneous initiation of the polymerization of MMA. 4. The biradicals can be the precursor of the radicals to form high-molecular-weight polymers. In future work, the other reactions of acrylates would be our focus to perfect the polymerization mechanism with the quantum mechanical tools.

Acknowledgements The authors wish to acknowledge the financial supports from the Scientific Research Fund of Hunan Provincial Education Department (No. 05A002), the National Natural Science Foundation of China (50675185) for the research work.

References

1. Günaydin H, Salman S, Tüzün NŞ, Avci D, Avıyente V (2005) J Int Quantum Chem 103:176–189
2. Jansen JFGA, Dias AA, Dorschu M, Coussens B (2002) Macromolecules 35:7529–7531
3. Wong MW, Radom L (1995) J Phys Chem 99:8582–8588
4. Spichty M, Giese B, Matsumoto A, Fischer H, Gescheidt G (2001) Macromolecules 34:723–726
5. Kamachi M (1987) Adv Polym Sci 82:207–275
6. Stickler M, Meyerhoff G (1978) Makromol Chem 179:2729–2745
7. Brand E, Stickler M, Meyerhoff G (1980) Makromol Chem 181:913–921
8. Lingnau J, Stickler M, Meyerhoff G (1980) J Eur Polym 16:785–791
9. Stickler M, Meyerhoff G (1981) Polymer 22:928–933
10. Lingnau J, Stickler M, Meyerhoff G (1983) Polymer 24:1473–1478
11. Lingnau J, Meyerhoff G (1984) Makromol Chem 185:587–600
12. Lingnau J, Meyerhoff G (1984) Macromolecules 17:941–945
13. Stickler M (1977) Ph.D. Thesis, Mainz
14. Clouet G, Chaumont P, Corpart P (1983) J Polym Sci A Polym Chem 31:2815–2824
15. Lehrle RS, Shortland A (1988) J Eur Polym 24:425–429
16. Nising P, Meyer T, Carloff R, Wicker M (2005) Macromol Mater Eng 290:311–318
17. McManus NT, Penlidis A, Dube MA (2002) Polymer 43:1607–1614
18. Cao G, Zhu Z, Zhang M, Yuan W (2004) J Appl Polym Sci 93:1519–1525
19. Khuong SK, Jones HW, Pryor WA, Houk KN (2005) J Am Chem Soc 127:1265–1277
20. Pryor WA, Lasswell LD (1975) Vol. V. Academic Press, New York
21. Flory PJ (1937) J Am Chem Soc 59:241–253
22. Mayo FR (1968) J Am Chem Soc 90:1289–1295
23. Mayo FR (1953) J Am Chem Soc 75:6133–6141
24. Lee C, Yang W, Parr RG (1988) Phys Rev B 37:785–789
25. Becke AD (1993) J Chem Phys 98:5648–5652
26. Becke AD (1988) Phys Rev A 38:3098–3100
27. Geerlings P, Proft FD, Langenaeker W (2003) Chem Rev 103:1793–1873
28. Becke AD (1996) J Chem Phys 104:1040–1046
29. Francl MM, Pietro WJ, Hehre WJ, Binkley JS, Defrees DJ, Pople JA, Gordon MS (1982) J Chem Phys 77:3654–3665
30. Panchenko A (2006) J Membr Sci 278:269–278
31. Fukui K (1981) Acc Chem Res 14:363–368
32. Gordon MH, Pople JA (1988) J Chem Phys 89:5777–5786
33. Merino P, Tejero T, Chiacchio U, Romeo G, Rescifina A (2007) Tetrahedron 63:1448–1458
34. Frisch MJ, Trucks GW, Schlegel HB, Scuseria GE, Robb MA, Cheeseman JR, Zakrzewski VG, MonTgomery JA Jr, Stratmann RE, Burant JC, Dapprich S, Millam JM, Daniels AD, Kudin KN, Strain MC, Farkas O, Tomasi J, Barone V, Cossi M, Cammi R, Mennucci B, Pomelli C, Adamo C, Clifford S, Ochterski J, Petersson GA, Ayala PY, Cui Q, Morokuma K, Malick DK, Rabuck AD, Raghavachari K, Foresman JB, Cioslowski J, Ortiz JV, Stefanov BB, Liu G, Liashenko A, Piskorz P, Komaromi I, Gomperts R, Martin RL, Fox DJ, Keith T, Al-Laham MA, Peng CY, Nanayakkara A, Gonzalez C, Challacombe M, Gill PMW, Johnson BG, Chen W, Wong MW, Andres JL, Head-Gordon M, Replogle ES, Pople JA (2003) Gaussian 2003W Revision B.05. Gaussian Inc, Pittsburgh PA
35. Valtazanos P, Elbert SF, Ruedenberg K (1986) J Am Chem Soc 108:3147–3149
36. Hirsch M, Quapp W, Heidrich D (1999) Phys Chem Chem Phys 1:5291–5299
37. Bartsch RA, Chae YM, Ham S, Birney DM (2001) J Am Chem Soc 123:7479–7486
38. Caramella P, Quadrelli P, Toma L (2002) J Am Chem Soc 124:1130–1131
39. Reyes MB, Lobkovsky EB, Carpenter BK (2002) J Am Chem Soc 124:641–651
40. Foresman JB, Frisch A (1996) Exploring chemistry with electronic. Gaussian Inc, Pittsburgh
41. Hess GH (1840) Bull Sci Acad Imp Sci (St. Petersburg) 8:257–272